Materials Letters: X 26 (2025) 100245

Contents lists available at ScienceDirect

Materials Letters: X

journal homepage: www.sciencedirect.com/journal/materials-letters-x

Surface contamination induced by warm severe surface peening using 100C6 steel and ZrO_2 shots

Y Austernaud [a,b,c], M Novelli [a,b,*], T.H. Kauffmann [d], P Bocher [c], T Grosdidier [a,b]

[a] Laboratoire d'Etude des Microstructures et de Mécanique des Matériaux (LEM3), UMR CNRS 7239, 7 rue Félix Savart, BP 15082, Metz F-57073, France
[b] LABoratoire d'Excellence Design des Alliages Métalliques pour Allègement des Structures (DAMAS), Université de Lorraine, Metz F-57045, France
[c] Laboratoire d'Optimisation des Procédés de Fabrication Avancés (LOPFA), Ecole de Technologie Supérieure 1100 rue notre dame Ouest H3C 1K3 Montréal, Canada
[d] Laboratoire Matériaux Optiques, Photonique et Systèmes (LMOPS), Université de Lorraine & Centrale Supélec, Metz 57070, France

ARTICLE INFO

Keywords:
Surface Mechanical Attrition Treatment (SMAT)
Warm Deformation
Surface contamination

ABSTRACT

The sample surface contamination induced during Surface Mechanical Attrition Treatment (SMAT) was studied after peening treatments carried out with 100C6 steel and ZrO_2 zirconia shots at room temperature, 523 K, and 773 K. All constituting parts of the treatment device (sonotrode, chamber, shots) contributed to sample surface contamination. Increasing the SMAT temperature led to a higher surface contamination with bigger contaminant debris as well as sample surface oxidation. In particular, several ZrO_2 shots were fragmented at 773 K due to a phase transformation embrittlement under warm condition.

1. Introduction

Mechanical surface treatments play a crucial role in enhancing material resistance such as fatigue and wear resistances. Among them, SMAT stands out for generating surface nanostructures and highly deformed gradients in the subsurface region [1,2]. However, Room Temperature (RT) SMAT has limitations, especially on high-strength materials, as increasing treatment energy and over processing generate surface cracks which are reducing fatigue resistance [3]. Thermally assisted surface treatments have been introduced to reduce flow stress and induce more plastic deformation. Elevating the processing temperature can also activate additional mechanisms such as dynamic recrystallization or dynamic precipitation, leading to the formation of novel microstructures [4,5]. In addition, SMAT is known to generate sample surface contamination, which can significantly affect corrosion [6,7] or diffusion as in the case of thermochemical duplex treatments leading to discontinuous nitrided layers [2,8]. As surface contamination can widely affect the surface properties, this study aims to investigate the contamination process occurring under SMAT, especially under warm peening conditions.

2. Material and methods

Cylindrical 316L stainless steel specimens (Ø6 mm, by 25 mm length) were subjected to SMAT (20 kHz, 60 µm, 10 min) at RT, 523 K, and 773 K. Ø2 mm 100C6 steel and Ø2.4 mm ZrO_2 yttria-stabilized zirconia (3Y-TZP) shots were used. They were set in motion by a titanium alloy sonotrode (Ti6Al4V) within a martensitic AISI 420 steel chamber. A schematic drawing of the warm treatment chamber together with the chemical compositions of the different constituting parts are given in Figs. 1S and Table 1S of the supplementary material as well as in [4]. For each temperature condition, SMAT using ZrO_2 shots was performed before the 100C6 one. New shots were used for each treatment and the chamber and sonotrode cleaned with ethanol. Raman spectroscopy was conducted three times on both the sample and shot surfaces using a Horiba LabRAM HR Evolution confocal microscope with a 532 nm Oxxius laser of 4 mW at 100X magnification for 20 s counting duration.

Surface chemical analyses were done by Energy-Dispersive X-ray Spectroscopy (EDS) using a ZEISS SUPRA 40 scanning electron microscope. As the SMAT device is composed of several parts having different chemical compositions (supplementary Table 1), characteristic chemical elements were chosen to trace the origin of the contamination. Ti and Zr were selected to trace contaminations from the sonotrode and ZrO_2

* Corresponding author at: Laboratoire d'Etude des Microstructures et de Mécanique des Matériaux (LEM3), UMR CNRS 7239, 7 rue Félix Savart, BP 15082, Metz F-57073, France.
E-mail address: marc.novelli@univ-lorraine.fr (M. Novelli).

https://doi.org/10.1016/j.mlblux.2025.100245
Received 8 April 2025; Received in revised form 23 May 2025; Accepted 29 May 2025
Available online 31 May 2025

shots, respectively. As the samples (17 % Cr, 10 % Ni), chamber (martensitic AISI 420: 12–14 % Cr) and the 100C6 shots (<1.7 % Cr) are all made of different steel grades, Ni was selected to identify the sample while Cr was selected for the chamber when it was not associated with Ni. Fe was selected for the shots when it was neither associated with Ni nor with a notable amount of Cr.

3. Results and discussion

Fig. 1(a-c) gathers optical images of the specimen surfaces and the associated Raman spectra (d-e) after SMAT at different temperatures using $Zr0_2$ and 100C6 shots. Depending on the selected deformation temperature, the specimen surfaces change in colour indicating modified oxidation states, Fig. 1(a-c). Among all the Raman acquisitions, Fig. 1(d-e), only the ones acquired on the samples SMATed at 773 K show clear identifiable peaks. Although the surface colour of samples SMATed at 523 K differs from the RT samples, the absence of spectra after SMAT at 523 K may be attributed to the thickness of the oxide layer which might be too thin to be detected. At 773 K, the Raman spectra are similar regardless of the shot materials. Most peaks correspond to hematite (Fe_2O_3), while the 663 cm^{-1} peak indicates magnetite (Fe_3O_4). Although Cr_2O_3 is the primary oxide in the native passive film of stainless steel, it is barely detected due to its low Raman sensitivity even if a weak band near 560 cm^{-1} may indicate Cr_2O_3. Signals at 510 and 640 cm^{-1} suggest TiO_2, but overlapping with Fe_2O_3 peaks makes identification uncertain, especially in specimens treated with steel shots where iron oxides dominate.

Fig. 2 shows the optical and Raman analyses of surfaces of the ZrO_2 and 100C6 shots. As seen in Fig. 2(a–c), the ZrO_2 shots become shinier due to metallization during SMAT. While they retained their spherical shape after RT treatment, several are fragmented after peening at 773 K. Raman spectra (Fig. 2(d)) acquired from different regions of the same surface of a shot used at 773 revealed both (i) peaks of the tetragonal ZrO_2 phase (spectrum 1) together with (ii) signals from Fe_2O_3 and Fe_3O_4 (spectrum 2), indicating surface contamination by iron oxides likely formed from the treated steel or chamber walls during high-temperature SMAT. Additional peaks at 178 and 382 cm^{-1}, associated with the monoclinic ZrO_2 phase and visible at room temperature, were further intensified with increasing peening temperature. A strain-induced tetragonal-to-monoclinic transformation in stabilized zirconia is considered beneficial, as the associated volume expansion at the crack tip helps to limit crack propagation [9]. Comparatively, when the phase transformation is thermally-induced, surface cracks leading to grain decohesion are formed as described in stabilized-zirconia during isothermal aging at 523 K [10]. Hence, the ZrO_2 shot toughness may be maintained during RT and 523 K SMAT by a transformation toughening mechanism whereas substantial shot fragmentation could be promoted by a thermal phase transformation at 773 K.

Concerning the 100C6 steel shots in Fig. 2(e-g), it is likely that the same surface metallization process took place during SMAT but the initial metallic aspect of the shots prevents it to be visible. The 100C6 shots kept their spherical shape and integrity for all SMAT temperature conditions. No distinct peaks are observed in the Raman spectra after SMAT at RT and 523 K, though changes in the baseline are evident. The flat baseline at RT may suggest the removal of a thin surface oxide layer, while the noisy baseline at 523 K likely results from surface oxidation, although it is impossible to identify specific oxides. At 773 K, characteristic peaks of Fe_2O_3 and Fe_3O_4 appear in the spectrum from the steel shot surface (Fig. 2(h)), with no clear evidence of titanium oxides.

Fig. 3 compares EDS chemical analyses of the sample surfaces after SMAT with ZrO_2 and 100C6 shots. The two samples treated at RT, Fig. 3 (a-b), show differing surface contamination states. The surface treated with ZrO_2 shots reveals a notable Ti and Zr contamination whereas the one treated with 100C6 shots does not have any. When the SMAT temperature is raised to 523 K, traces of Ti are present on the sample surfaces for both shots. In addition, Zr is detected when ZrO_2 shots are used and areas rich in Fe are observable after the use of 100C6 steel shots. Peening at 773 K with ZrO_2 shots, Fig. 3(e), results in more evident Ti contamination and Zr chunks (about 200 μm in Fig. 3(e)) were found encrusted at the sample surface. Chamber contamination is also visible as (Fe, Cr) speckles, as seen within the red dotted circle near the Zr incrustation in Fig. 3(e). The use of 100C6 shots at 773 K, Fig. 3(f), reveals Fe contamination from the shots (red circles) and from the treatment chamber (Fe, Cr rich areas – red dotted circles).Although the chamber and sonotrode were cleaned between treatments, fine zirconia residues were still observed after SMAT with steel shots at 773 K (Fig. 3f), indicating that only the shots can act as contamination carriers as confirmed by EDS analysis of the shot surfaces (Fig. 2S, Supplementary Material). As with the samples, shot contamination increased with SMAT temperature. (Ni, Cr)-rich regions from the sample were also

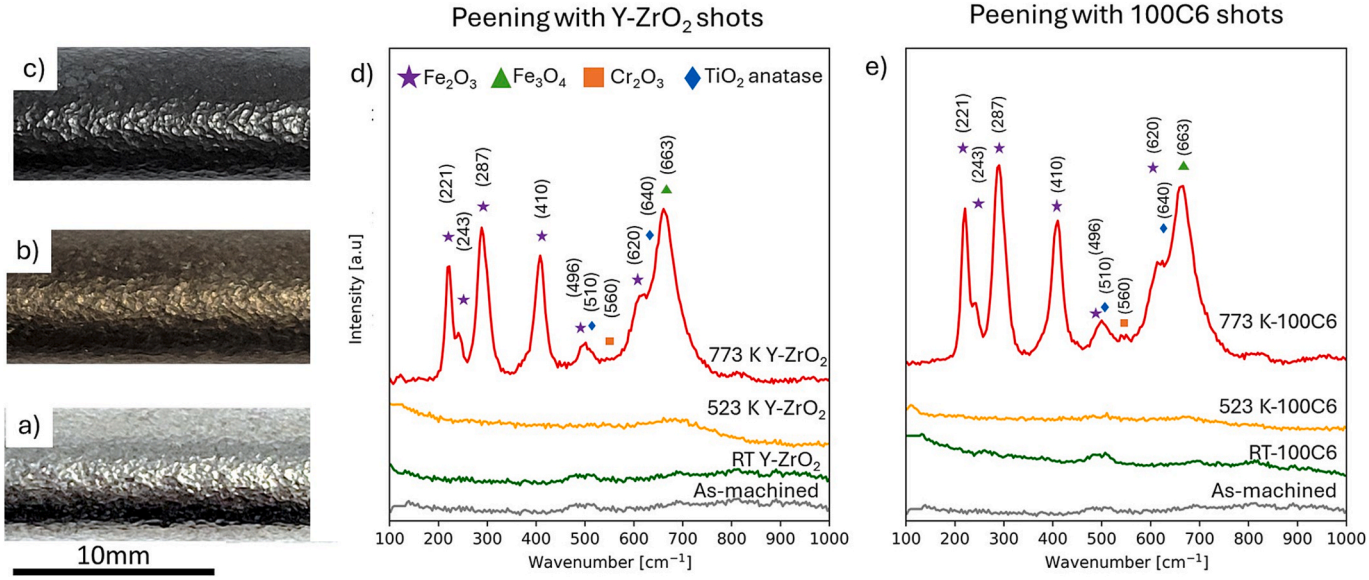

Fig. 1. (a–c) Optical observations of the sample surfaces after SMAT at (a) RT, (b) 523 K, and (c) 773 K. All the images share the same scale. (d–e) Raman spectra acquired on sample surfaces after SMAT at RT (green), 523 K (orange), and 773 K (red), using (d) Y-ZrO_2 and (e) 100C6 shots. (For interpretation of the references to colour in this figure legend, the reader is referred to the web version of this article.)

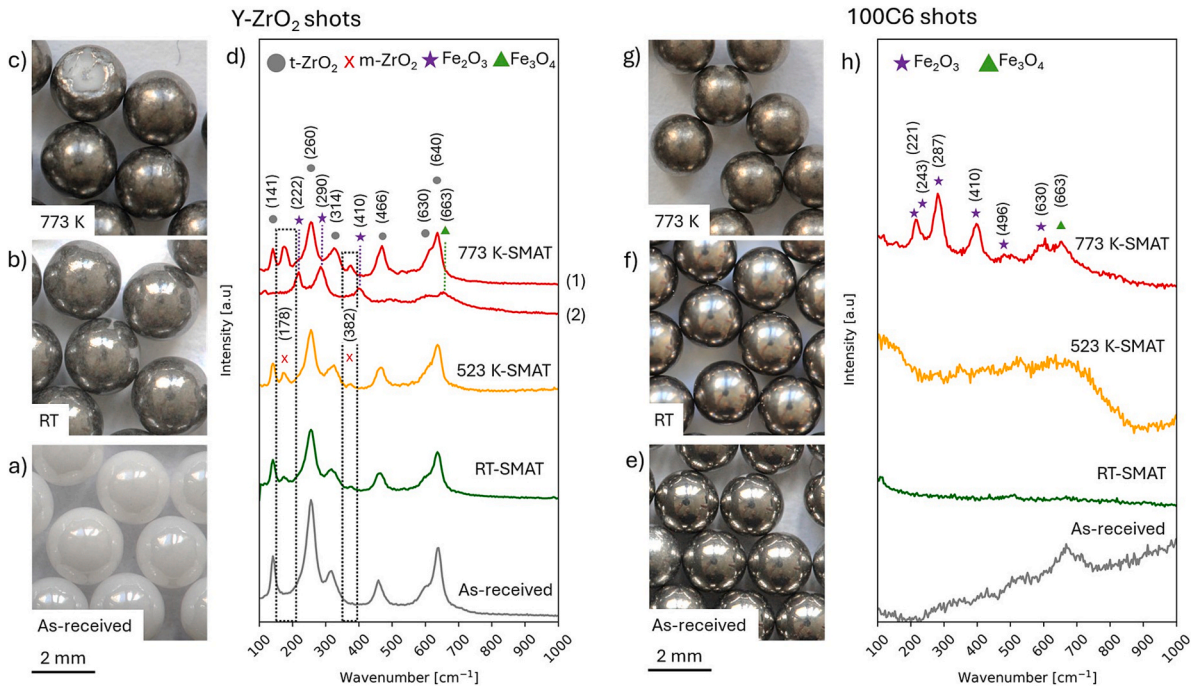

Fig. 2. Optical images of (a–c) ZrO_2 shots and (e–g) 100C6 steel shots in the (a, e) as-received condition, (b, f) after RT SMAT, and (c, g) after 773 K SMAT. (d, h) Raman spectra acquired from the shot surfaces after SMAT at RT (green), 523 K (orange), and 773 K (red). In (d), both spectra were acquired from the same ZrO_2 shot surface at different locations: spectrum 1 shows characteristic ZrO_2 peaks, while spectrum 2 reveals additional Fe_2O_3 and Fe_3O_4 peaks. (For interpretation of the references to colour in this figure legend, the reader is referred to the web version of this article.)

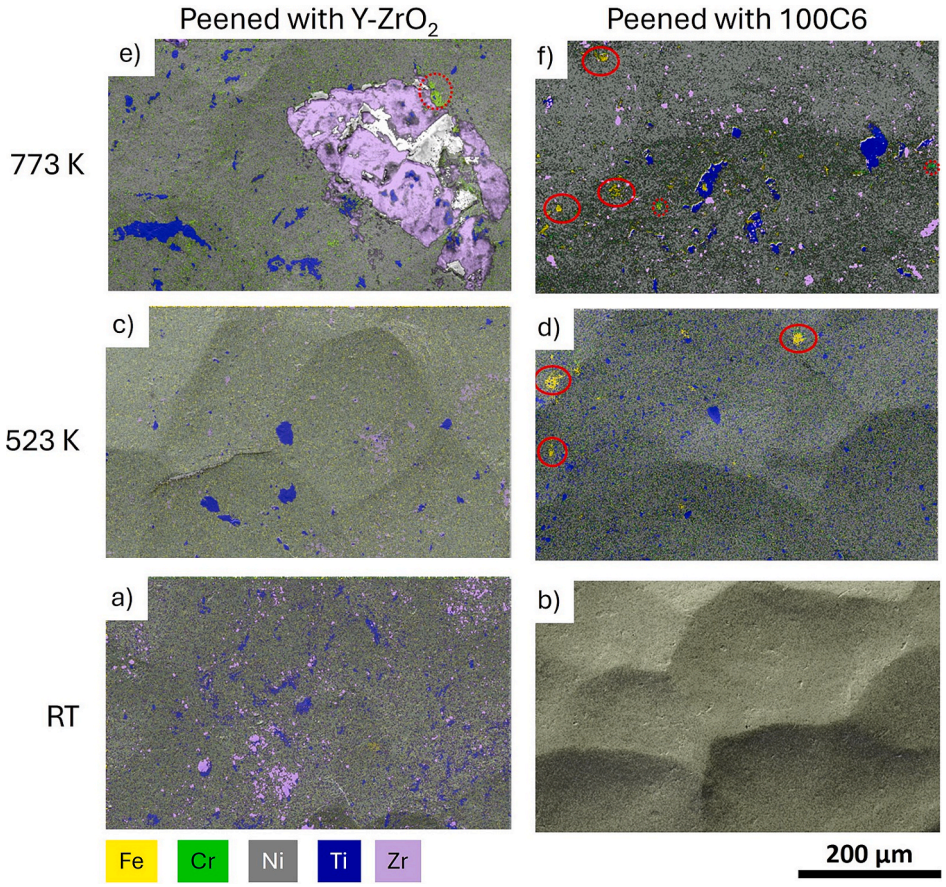

Fig. 3. EDS acquisitions of the sample surfaces after SMAT using (a, c, e) ZrO_2 and (b, d, f) 100C6 shots at (a, b) RT, (c, d) 523 K and, (e, f) 773 K.

found on the shot surfaces after SMAT at 773 K. The Zr contamination on 100C6-peened surfaces (Fig. 3f) likely results from ZrO_2 debris, previously embedded in the chamber or sonotrode, being transferred to the 100C6 shots and then to the sample.

4. Conclusion

SMAT was performed at RT and elevated temperatures using ZrO_2 or 100C6 shots. Investigations showed that all the parts constituting the SMAT machine device are involved in the sample surface contamination process. Warm conditions tend to increase the surface contamination, especially by Ti coming from the sonotrode, and lead to the oxidation of the sample surface at 773 K. A particular attention has to be taken when using ZrO_2 shots under warm conditions as an embrittling tetragonal → monoclinic phase transformation induce shot fragmentation.

CRediT authorship contribution statement

Y Austernaud: Writing – review & editing, Writing – original draft, Methodology, Investigation, Conceptualization. **M Novelli:** Writing – review & editing, Writing – original draft, Supervision, Conceptualization. **T.H. Kauffmann:** Writing – review & editing, Investigation, Data curation. **P Bocher:** Writing – review & editing, Supervision, Conceptualization. **T Grosdidier:** Writing – review & editing, Supervision, Conceptualization.

Declaration of competing interest

The authors declare that they have no known competing financial interests or personal relationships that could have appeared to influence the work reported in this paper.

Acknowledgements

This study was supported in part by the French Government through the program "Investment in the future" operated by the National Research Agency (ANR) and referenced by ANR-11- LABX-0008-01 (Labex DAMAS). The SMATs and electronic observations were carried out on the Procédés and MicroMat platforms of LEM3, University de Lorraine, respectively. Raman spectroscopy was carried out at the Spectroscopy Platform of the LMOPS, Université de Lorraine & CentraleSupélec.

Appendix A. Supplementary data

Supplementary data to this article can be found online at https://doi.org/10.1016/j.mlblux.2025.100245.

Data availability

Data will be made available on request.

References

[1] T.O. Olugbade, J. Lu, Nano Mater. Sci. 2 (1) (2020) 3–31, https://doi.org/10.1016/j.nanoms.2020.04.002.
[2] T. Grosdidier, M. Novelli, Mater. Trans. 60 (7) (2019) 1344–1355, https://doi.org/10.2320/matertrans.MF201929.
[3] E. Maleki, S. Bagherifard, O. Unal, M. Bandini, G.H. Farrahi, M. Guagliano, Sci. Rep. 11 (1) (2021) 22035, https://doi.org/10.1038/s41598-021-01152-2.
[4] Y. Austernaud, M. Novelli, P. Bocher, T. Grosdider, J. Mater. Process. Technol. 339 (2025) 118824, https://doi.org/10.1016/j.jmatprotec.2025.118823.
[5] J. Liu, C. Ye, Y. Dong, Adv. Ind. Manuf. Eng. 2 (2021) 100006, https://doi.org/10.1016/j.aime.2020.100006.
[6] D. Fabijanic, A. Taylor, K.D. Ralston, M.X. Zhang, N. Birbilis, Corrosion 69 (6) (2013) 527–535, https://doi.org/10.5006/0763.
[7] L. Wen, Y. Wang, Y. Jin, X. Ren, Corros. Eng. Sci. Technol. 50 (6) (2015) 425–432, https://doi.org/10.1179/1743278214Y.0000000239.
[8] Y. Samih, M. Novelli, T. Thiriet, B. Bolle, N. Allain, J.J. Fundenberger, G. Marcos, T. Czerwiec, T. Grosdidier, IOP Conf Ser. Mater. Sci. Eng. 63 (1) (2014) 012020, https://doi.org/10.1088/1757-899X/63/1/012020.
[9] T.K. Gupta, F.F. Lange, J.H. Bechtold, J. Mater. Sci. 13 (1978) 1464–1470, https://doi.org/10.1007/BF00553200.
[10] L. Jong-Kook, K. Hwan, J. Mater. Sci. 29 (1994) 136–140, https://doi.org/10.1007/BF00356584.